https://doi.org/10.32604/zkg.2026.077196

ARTICLE

Enhancing the properties of artificial aggregate prepared with excavated soil and alkali-activated slag through thermal curing and surface treatment

Shu Liu[1,2], Weixin Zhang[2], Yuguang Wang[2], Fangying Wang[3], Xiaojian Yu[4], Binmeng Chen[5] and Bo Li[2,*]
[1]Nottingham Ningbo China Beacons of Excellence Research and Innovation Institute, University of Nottingham Ningbo China, Ningbo, China
[2]Department of Civil Engineering, University of Nottingham Ningbo China, 199 Taikang East Road, Ningbo, China
[3]Department of Civil Engineering and Management, University of Manchester, Manchester, UK
[4]Ningbo Communication Engineering Construction Group Co., Ltd., Ningbo, China
[5]Institute of Applied Physics and Materials Engineering, University of Macau, Macao, China
*Corresponding Author: Bo Li. Email: bo.li@nottingham.edu.cn

Received: 04 December 2025; Accepted: 21 January 2026

ABSTRACT: The widespread application of alkali-activated soil-based artificial aggregates (AAs) is limited by their low early strength and high-water absorption, creating an imperative for effective enhancement methods. This study investigates the efficacy of thermal treatments (heat curing and microwave curing) and surface treatments (alkaline solution immersion, double pelletisation, and slurry immersion) in enhancing their performances. The properties of AAs were evaluated through crushing strength, water absorption, and apparent density tests, with underlying mechanisms elucidated by microstructural analyses. The results demonstrate that both heat curing and microwave curing significantly enhance the early-age strength, improving the 1-day crushing strength by over 140% and 100%, respectively. This enhancement is attributed to the accelerated formation of C-(A)-S-H gels and hydrotalcite. However, a slight increase in water absorption and a reduction in 28-day crushing strength are observed, primarily due to microcracking induced by the rapid drying process. Among the surface treatments, alkaline solution immersion and double pelletisation increase apparent density by ~3.6%, reduce water absorption by ~22.3%, and enhance crushing strength by ~30.9%, primarily due to the formation of a denser outer shell. In contrast, slurry immersion adversely affects the properties owing to its uneven coating and potential aggregate swelling. This study provides practical strategies and mechanistic insights for optimising the performance of AAs, facilitating their industrial production and application.

KEYWORDS: Alkali-activated soil-based artificial aggregate; heat curing; microwave curing; alkaline solution immersion; slurry immersion; double pelletisation

MATERIALS

1 Introduction

Aggregates, constituting 60%–70% volume of concrete, have an essential impact on the mechanical properties and durability of concrete [1]. While traditional aggregates are predominantly derived from natural crushed stone, the overexploitation of these non-renewable resources has imposed severe strains on the ecological environment [2]. In response to this pressing sustainability challenge, recycled aggregates and artificial aggregates (AAs) have emerged as promising alternatives in modern concrete production [3]. Among them, AAs stand out with distinct advantages due to their low density and porous structure. This reduces the self-weight of concrete [4] and is conducive to improving the thermal and sound insulation performances of concrete [5, 6]. Most notably, they can be prepared using various solid wastes, embodying environmental protection and resource recycling value [7], which has made them a key research hotspot in recent years.

AAs can be primarily classified into thermally processed and cold-bonded types based on their production methods [8]. The cold-bonding method involves agglomerating raw materials with binders at ambient temperature, followed by a curing process. This technique is characterised by its low energy consumption, minimal pollutant emissions, and cost-effectiveness [7]. Several formulations for cold-bonded aggregates utilising different solid wastes have been proposed

in the literature. For instance, Ibrahim et al. [9] produced cold-bonded AAs using cement, Ground Granulated Blast-furnace Slag (GGBS), and quartz, and reported a 28-day strength ranging from 0.27 to 1.04 MPa, densities between 652.18 and 1114.42 kg/m^3, and water absorption rates of 15.83~28.52%. Similarly, Tian et al. [10] employed fly ash and red mud to fabricate AAs via cold-bonding technology, resulting in a water absorption of 9.8%~12.1% and a 28-day strength of 1.46~6.18 MPa. Incinerator bottom ash (IBA) derived from municipal sewage sludge was also adopted as the raw material for cold-bonded aggregate production under an alkaline activation system, with a water absorption of 4.74~7.08% and a cylindrical compressive strength of 0.62~1.86 MPa [11]. Furthermore, Zhou et al. [12] prepared alkali-activated AAs using lithium slag and GGBS, achieving a cylindrical compressive strength of 6.9 MPa. It is worth noting that most existing studies have focused on aggregates produced from reactive solid wastes (e.g., GGBS, fly ash, IBA, etc.). In contrast, the authors of this paper [13] developed AAs using inert waste soil with the alkali-activation method. The primary rationale is that large volumes of waste soil are generated during construction activities; however, its lack of reactivity presents substantial challenges to high-value resource utilisation. The authors' previous work has provided a viable pathway for the efficient utilisation of the waste soil. With the soil content ranging from 60% to 90%, the developed AAs achieve a 28-day crushing strength of 1.71~8.98 MPa, water absorption of 9.5%~15.9%, and density of 1604~1863 kg/m^3. Notably, while a significant progress has been made in the preparation and performance characterisation of AAs, their widespread practical application still faces key challenges such as insufficient early-age strength development and high-water absorption.

Heat curing can efficiently enhance the early strength of cementitious materials or alkali-activated materials by accelerating the hydration process [14, 15]. For cold-bonded AAs, most of them were cured at ambient temperature (20°C) and 95% relative humidity in the literature, though some studies have explored heat-curing effects on their properties. For example, Shivaprasad et al. [16] reported that curing alkali-activated fly ash aggregates at 80°C for 24 h increases their 14-day strength from 2.4 MPa to 3.1 MPa. Furthermore, Shivaprasad et al. [17] found that higher temperatures and longer curing durations enhance the crushing strength of fly ash-based AAs by up to 40% but significantly increase their water absorption by 87.8%. In other words, heat curing can improve early strength but exerts a negative impact on water absorption. Moreover, the adverse effects of heat curing may also extend to long-term strength. For example, Chen et al. [18] found that alkali-activated slag mortars cured at 60°C for 3, 6, 12, and 24 h have 1-day compressive strengths that are 29.0%, 35.6%, 47.0%, and 51.1% higher than those of ambient-cured samples, respectively. However, heat curing has a negative impact on their 28-day strengths. This could be attributed to the rapid formation of reaction products encapsulating precursor particles, hindering their dissolution and further reaction [19, 20]. Another reason could be that heat curing accelerates the evaporation of free water in the matrix, disrupting the continuous hydration of cementitious materials [21]. Moreover, high-temperature curing can also lead to the formation of microcracks and a coarser pore structure, which may also negatively impact long-term durability [22]. Therefore, the positive and negative impacts of adopting heat curing for AAs must be considered comprehensively. In addition, the impact of heat curing varies significantly depending on the reaction system, product size, and shape [23, 24]. The AAs developed by the authors previously [13], which are characterised by their high inert component content (60%~90%), also have a clear demand for performance enhancement. However, it remains uncertain whether heat curing can effectively improve their early strength without significantly affecting their long-term strength and water absorption adversely, which requires further studies.

Beyond conventional heat curing, microwave curing has emerged as a promising alternative with unique advantages, including shorter irradiation duration, lower heat energy loss, and higher energy efficiency. This is because microwave irradiation achieves more uniform and effective heating by penetrating the sample, whereas traditional heat curing only warms the surface [19]. For example, El-Feky et al. [20] reported that alkali-activated slag samples irradiated with 720 W microwaves for 2 min reach ~90% of their 28-day crushing strength at 7 days. Guan et al. [25] found that microwave curing can significantly reduce the final setting time from 7 h at room temperature to 10 min under 119 W microwave curing, while barely affecting their final compressive strength after curing. However, some researchers have also pointed out potential negative effects of microwave curing for cementitious materials. For example, Lam et al. [26] indicated that although microwave curing can significantly boost early-stage strength of concrete, the long-term strength may decline. A similar conclusion was also reported in Zhou et al. [27]. Li et al. [28] mentioned that higher power and temperature settings can cause an increase in the crystallisation of hydration products and the proportion of harmful pores, which fundamentally damages the microstructure. Thus, like heat curing, microwave curing exhibits both merits and drawbacks, and its effects on the developed alkali-activated excavated soil-based AAs require further investigation.

Most AAs are porous and contain air voids, resulting in a higher water absorption rate than

natural aggregates [29–31]. This high-water absorption can be mitigated by applying various surface treatment methods. One primary method is slurry immersion, which involves immersing the aggregates in a cementitious or pozzolanic slurry. For instance, Siletani et al. [32] reported that after 12–24 h of immersion in different pozzolanic slurries, the water absorption of recycled aggregate is reduced from 6.5% to a minimum of 4.7%. Similarly, Dixit et al. [33] treated calcined lightweight AAs with silica fume (SF) and fly ash (FA) slurries and found that their water absorption was reduced from 27.6% to 17.5% with SF soaking and to 24.9% with FA soaking. The water absorption of the AAs can be further reduced to a minimum of 9.3% with multiple coatings. Meanwhile, the compressive strength was enhanced by 27.2% and 24.4% for FA and SF soaking, respectively. Another prominent technique is double pelletisation, where fresh aggregates are pelletised with a binder for a second time [34, 35]. Ferraro et al. [36] reported that double pelletisation with cement and marble sludge for fly ash-based AAs can reduce water absorption by up to 55% and improve crushing strength by up to 5.7 times. Colangelo [34] also reported that double pelletisation could reduce the water absorption of fly-ash aggregate by around 20%. A third approach, specifically for alkali-activated aggregates, is alkaline activator immersion. This process involves immersing the aggregates in an alkaline solution for about 30 min to one hour. Gesoğlu et al. [37] reported that this treatment decreases the water absorption of fly ash aggregates by about 88% (from 27% to 3%) and increases the crushing strength by 100%. Similar enhancements have also been documented in other studies [38, 39]. In summary, these three surface treatment methods have demonstrated considerable feasibility for enhancing various properties of AAs. However, their effectiveness depends on factors such as the aggregate intrinsic composition, the specific reaction system, the type of treatment materials used, and processing parameters. Based on this knowledge, applying these existing surface treatment strategies to alkali-activated soil-based aggregates developed by the authors [13] represents a critical next step and requires further systematic investigation.

In summary, the widespread use of AAs is restricted by their low early strength and high-water absorption, requiring effective enhancement methods, whereas the effects of heat/microwave curing and surface modification strategies remain unclear. Therefore, the present work extends the previous study [13], which established the baseline formulation for alkali-activated soil-based AAs incorporating 70% inert solid wastes. The current research aims to enhance the early strength and reduce the water absorption of alkali-activated soil-based AAs. The effectiveness of two curing regimes (heat curing and microwave curing) and three surface treatment methods (alkaline activator immersion, alkali-activated GGBS slurry immersion, and double pelletisation) is evaluated by testing the apparent density, water absorption, and crushing strength of AAs at various ages. Additionally, the underlying mechanisms are investigated in combination with Thermogravimetric Analysis (TGA), Scanning Electron Microscopy (SEM), and microhardness tests. The findings of this research are expected to provide valuable insights into optimising the performance of alkali-activated soil-based AAs and offer practical solutions for their production.

2 Experimental programme

To evaluate the effects of curing enhancement and surface treatment on the properties of the AAs, the overall research plan is illustrated in Figure 1.

In this study, the mix proportion specified in Liu et al. [13] is selected as the control group. Specifically, Excavated Soil (ES) and GGBS are mixed at a mass ratio of 70:30, and the alkali dosage and silicate modulus are 6% (weight of the solid) and 1.0, respectively. The water-to-solid mass ratio is fixed at 0.18. The control group is

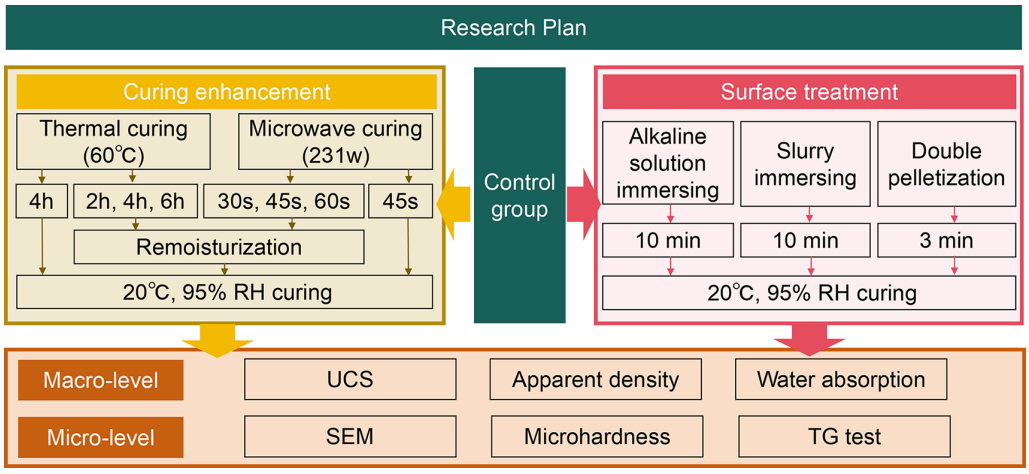

Figure 1 Overall research plan

cured at 20°C and 95% relative humidity (RH) until the targeted curing age.

Regarding the curing enhancement methods, heating curing and microwave curing regimes are considered in the current work. Details of the methods are given in Section 2.3. The surface treatment methods comprise alkaline solution immersion, slurry immersion, and double pelletisation. Detailed descriptions of these techniques are provided in Section 2.4. To evaluate the effectiveness of these methods, the crushing strength, apparent density, and water absorption of the AAs are measured and compared. In addition, microstructural analyses, including SEM, microhardness testing, and TGA, are conducted to elucidate the underlying mechanisms of the enhancement methods.

2.1 Raw materials

The raw materials involved in this study primarily include ES, GGBS, and an alkaline activator prepared with water glass, sodium hydroxide, and water. The ES was obtained from a construction site in Ningbo, China, specifically as waste soil generated during the drilling and pouring of bored piles for highway construction. Its particle size distribution, as shown in Figure 2, classifies it as clay in accordance with BS ISO EN 14688–2

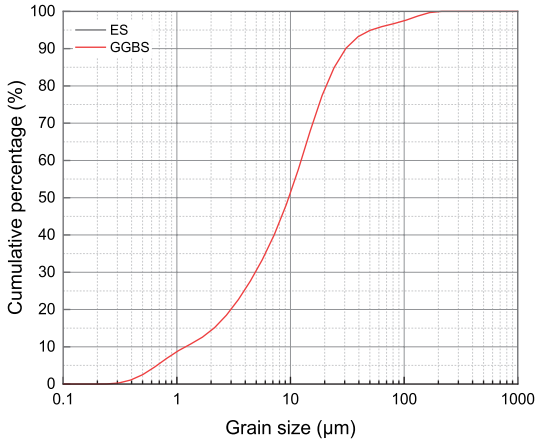

Figure 2 Particle size distribution of the ES and GGBS [13]

[40]. The waste soil exhibits a high initial moisture content, but it is dried in this study prior to being used for AA preparation. The specific gravity of ES is 2.11. Previous X-ray Diffraction (XRD)/TGA analyses [13] indicate that ES mainly consists of the crystalline phases illite, quartz, albite, and calcite, with its chemical compositions detailed in Table 1.

The GGBS utilised in this work was sourced from Lingshou Yanxing Mineral Products Processing Factory. It has a specific gravity of 2.92, and its particle size distribution is presented in Figure 2. Compared to ES, GGBS displays a finer particle size distribution. According to previous XRD/TGA results [13], its main component is calcium oxide, with its chemical composition provided in Table 1.

Table 1 Chemical constituents of the ES and GGBS [13]

Compound	Composition (%)	
	ES	GGBS
Na_2O	0.588	0.155
MgO	2.528	7.415
Al_2O_3	16.316	13.795
SiO_2	63.341	26.963
SO_3	0.085	3.748
K_2O	3.226	0.325
CaO	4.868	44.867
TiO_2	1.062	1.465
Fe_2O_3	7.035	0.369

The alkaline activator was developed by integrating three core components, including water glass, sodium hydroxide pellets, and deionised water. The water glass has a mass-based chemical composition of 26.8% silicon dioxide (SiO_2), 8.3% sodium oxide (Na_2O), and 64.9% water (H_2O), and the sodium hydroxide has a purity exceeding 98%.

2.2 Artificial aggregate preparation

The alkali-activated AAs were prepared according to the procedure illustrated in Figure 3. Initially, dried ES and GGBS (mass ratio = 70:30) were mixed in a low-speed blender for 5 min. Subsequently, the alkaline activator was prepared by mixing Na_2O, water glass, and water. The solution was manually stirred until complete dissolution was achieved, followed by sealing and cooling. For the pelletisation process, both the solid powders (i.e., ES and GGBS) and the alkaline activator were divided into two equal batches. The first batch of solid powder was loaded into the pelletiser, and the first batch of activator was gradually sprayed onto it over a period of 3 min. The second batch of powder was then introduced, and the spraying process (3 min) was repeated with the remaining solution to produce the green aggregates. The AAs in the control group were cured by sealing them in plastic bags and storing them at 20°C and 95% relative humidity for the target days. For the other groups considering different curing enhancement or surface treatment methods, the details of these methods are provided in Sections 2.3 and 2.4.

2.3 Curing enhancement regime

In the present work, two curing enhancement regimes were considered. The first regime involves subjecting fresh aggregates to short-term heat curing to enhance their early-age strength before transferring them to a temperature-controlled chamber at 20°C for subsequent curing. Specifically, an in-bath heating method was adopted in this study: the fresh aggregates were sealed with plastic film and placed into a water bath maintained

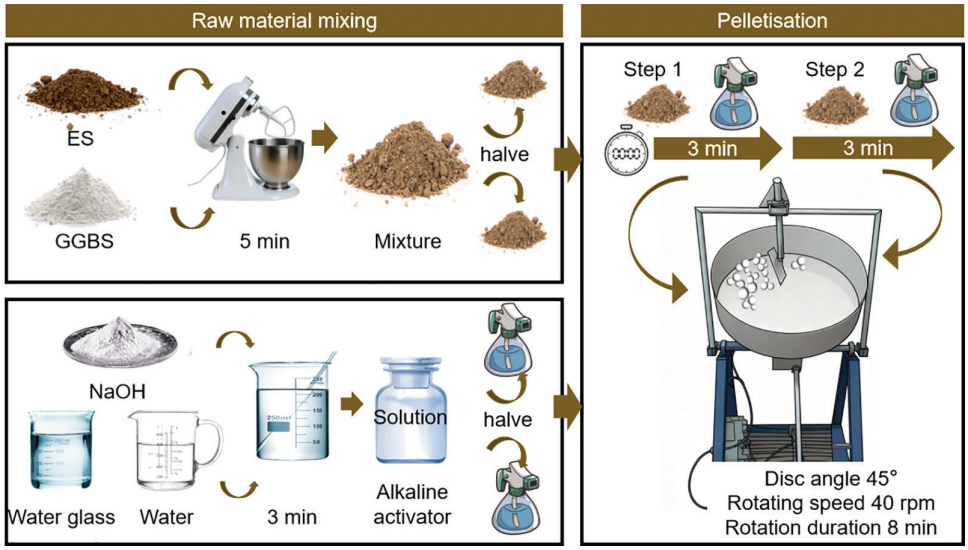

Figure 3 Flow-chart of artificial aggregate preparation

at 60°C for 2, 4, or 6 h. This temperature (60°C) is generally regarded as the optimal temperature for the alkali-activated slag system [41]. Upon completion of the pre-set heat curing duration, the aggregates were transferred to a temperature-controlled chamber at 20°C for curing. Notably, previous studies have mentioned that heat curing may accelerate the evaporation of internal free water in aggregates, which could adversely affect the development of aggregate strength. To mitigate this adverse effect, a supplementary re-moisturisation process was also applied for the heat-cured AAs. Specifically, the AAs were re-moisturised by immersing them in water for a few seconds. They were then wiped with a dry towel until no excess water remained on the aggregates. The re-moisturised aggregates were stored under sealed conditions at 20°C until testing.

Similarly, microwave curing was adopted as an alternative enhancement method in this study. The procedure was largely consistent with the heat-curing method, but a 231 W microwave oven was used to replace the water bath, with irradiation durations set at 30, 45, and 60 s to investigate their effects on the properties of the AAs. The effect of re-moisturisation is also considered for microwave-cured AAs.

The detailed research plan considering different curing enhancement regimes is listed in Table 2.

2.4 Surface treatment methods

Three surface treatment methods were adopted for enhancing the properties of AAs, as shown in Figure 4. For the alkaline solution immersion and slurry immersion processes, the fresh aggregates were submerged in an alkaline solution or an alkali-activated slag slurry for 10 min [7, 42]. Here, the alkaline activator has an alkali dosage of 10% and a silicate modulus of 1.0. The slurry was prepared with slag activated with an alkali dosage of 6%, a silicate modulus of 1.0, and a water-to-powder ratio of 0.5. Subsequently, the treated aggregates were transferred to a sieving machine equipped with a 2.36 mm sieve for 1 h to remove the excess alkaline solution or slurry on the aggregate surface. Afterwards, the treated aggregate was sealed and cured at 20°C and 95% relative humidity for 28 days.

For double palletisation method, the second pelletisation was carried out immediately after the initial pelletisation. An additional 10 wt% of GGBS powder (relative to the original mixed powder) was added to the pelletising disc at the start of the second pelletisation stage, which lasts 3 min.

Table 2 Details of curing regimes used for AAs

Group ID	Curing Regimes	Curing Duration	Curing Temp./Microwave Power	Additional Method
Control group	Standard curing (SC)	28 day	20°C	–
HC-60-4	Heat curing (HC) + SC	1 d, 3 d, 28 d (incl. 4 h HC)	60°C	–
HC-60-2-re		1 d, 3 d, 28 d (incl. 2 h HC)		Re-moisturisation
HC-60-4-re		1 d, 3 d, 28 d (incl. 4 h HC)		Re-moisturisation
HC-60-6-re		1 d, 3 d, 28 d (incl. 6 h HC)		Re-moisturisation
MW-231-45	Microwave curing (MC) + SC	1 d, 3 d, 28 d (incl. 45 s MC)	231 W	–
MW-231-30-re		1 d, 3 d, 28 d (incl. 30 s MC)		Re-moisturisation
MW-231-45-re		1 d, 3 d, 28 d (incl. 45 s MC)		Re-moisturisation
MW-231-60-re		1 d, 3 d, 28 d (incl. 60 s MC)		Re-moisturisation

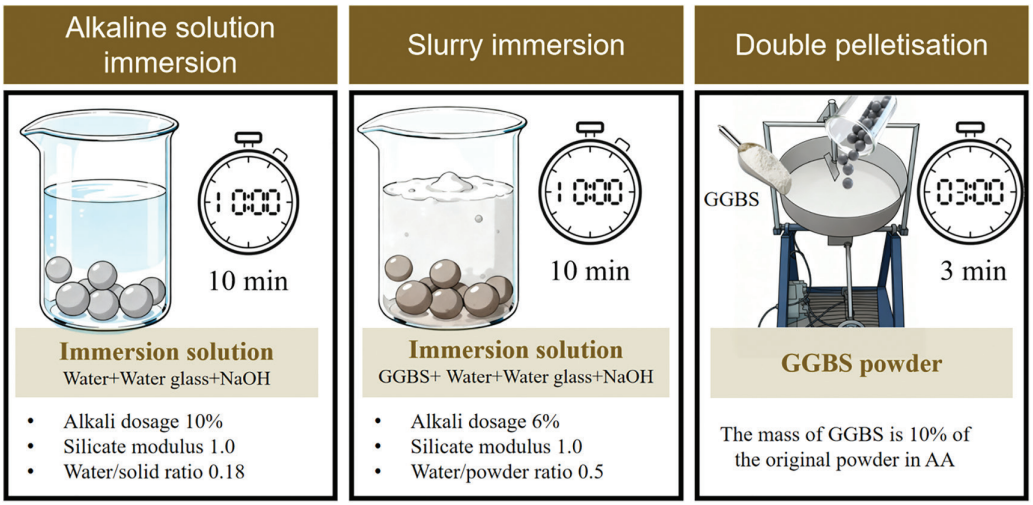

Figure 4 Surface treatment methods for AAs

2.5 Testing methods

2.5.1 Apparent density

The oven-dried apparent density of the hardened AAs was determined following GB/T 17431.2–2010 [43]. A 300 g sample (m), after being oven-dried to a constant mass, was re-saturated, surface-dried with a towel, and placed into a measuring cylinder with 500 mL of water for volume measurement (V). The apparent density (D_o) can be calculated as Equation (1). More details about this measurement method can be found in Liu et al. [13]. Each test was repeated twice until the deviation was less than 2%.

$$D_o = (m/V - 500) \times 1000 \quad (1)$$

2.5.2 Water absorption

Water absorption of the AAs was measured in accordance with GB/T 17431.2–2010 [43]. Both 1-h and 24-h water absorption values (denoted as $W_{a\text{-}1h}$ and $W_{a\text{-}24h}$) were determined. The hardened AAs were first oven-dried at 105°C until a constant mass was achieved. For each test, approximately 300 g of oven-dried aggregate was weighed, and the mass was recorded as m_1. The sample was then immersed in water for either 1 h or 24 h. After the specified immersion time, the aggregate was removed, surface-dried with a towel, and weighed again; the mass was recorded as m_2 (for 1 h) and m_3 (for 24 h). $W_{a\text{-}1h}$ and $W_{a\text{-}24h}$ were then calculated using Equations (2) and (3), respectively. Each test was repeated three times, and the average value was reported.

$$W_{a\text{-}1h} = ((m_2 - m_1)/m_2) \times 100\% \quad (2)$$

$$W_{a\text{-}24h} = ((m_3 - m_1)/m_3) \times 100\% \quad (3)$$

2.5.3 Crushing strength

Referring to previous studies [13], the crushing strength of AAs was measured by a universal testing machine with a loading capacity of 50 kN and ±0.5% relative error range. The loading rate was 0.6 mm/min [7, 18]. The peak load (P) and the vertical distance (H) between the upper plate and the bottom plate at the initial state were recorded. The crushing strength (S_c) can be calculated with Equation (4) [44].

$$S_c = (2.8 \times P)/(3.14 \times H^2) \quad (4)$$

For each group of tests, 12 aggregate particles with sizes between 10~12 mm were tested, and the average value was calculated.

2.5.4 Thermogravimetric analyses

TGA was conducted to characterise the thermal decomposition of the AA samples in the present work. The cured samples were treated by immersion in isopropanol for over 24 h to remove free water and terminate hydration, followed by vacuum drying at 20°C for three days to remove the solvent. The dried AAs were then ground and sieved through a 75 µm mesh to obtain the powder [45]. For each test, approximately 50 mg of this powder was heated from 30°C to 1000°C at 10°C/min under a 50 mL/min nitrogen flow [46].

2.5.5 Scanning electron microscopy

The microstructural morphology of the AA samples was examined using SEM. The hardened aggregate was immersed in isopropanol for over 24 h to stop hydration and then vacuum-dried at 20°C for three days. Half of an aggregate was then impregnated and mounted in epoxy resin within a rubber mould measuring 25 mm in diameter and 20 mm in height. The mounted samples were polished using a Buehler AutoMet 250 polisher with a sequential series of diamond and silica suspensions: 9 µm, 3 µm, 0.5 µm, 0.05 µm and 0.025 µm [47]. A photograph of the impregnated aggregates is presented in Figure 5. Prior to SEM observation, the prepared samples were fixed onto a specimen stub and coated with a 5 nm thick gold layer using a sputter coater. Microstructural analysis was subsequently performed by acquiring backscattered electron images.

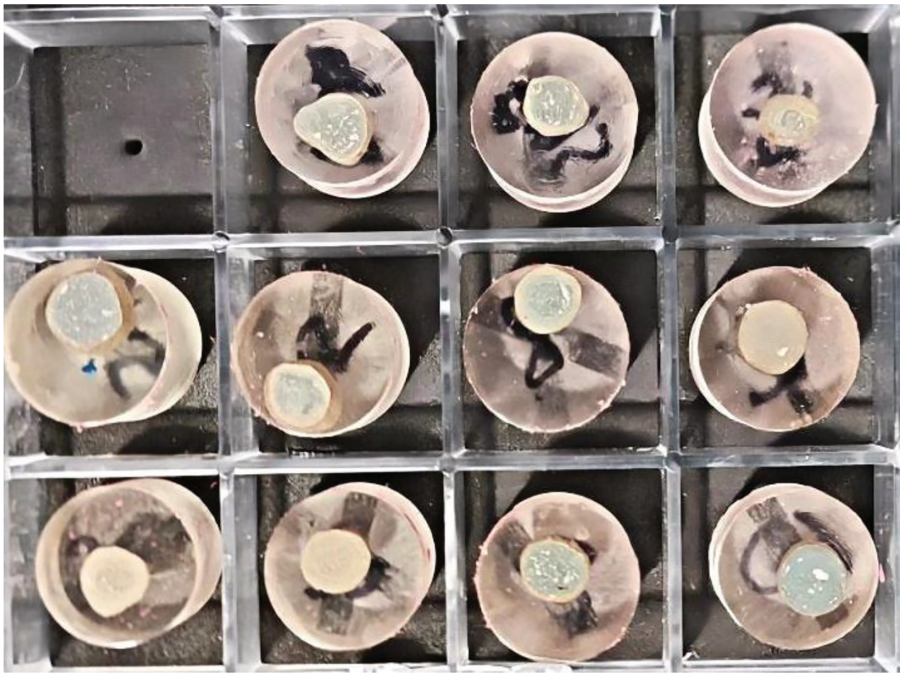

Figure 5 Aggregate samples for SEM observation

2.5.6 Microhardness

The microhardness distribution from the outer shell to the inner core of the surface-treated aggregates was characterised using a digital Vickers microhardness tester (HVX-1000A). Tests were performed on the cross-sections of the polished aggregate samples prepared in Section 2.5.5. Indentations were made at a total of 13 points, as illustrated in Figure 6. A load of 10 g and a dwell time of 10 s were applied for each measurement.

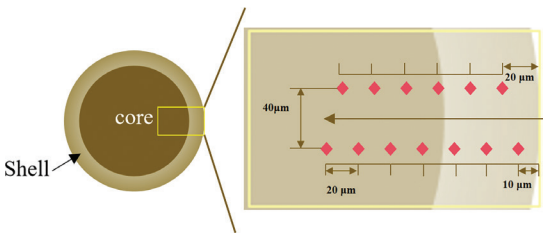

Figure 6 Microhardness indentation pattern for AAs

This procedure was repeated three times for each sample to ensure statistical reliability, and the average values were calculated.

3 Results and discussion

3.1 Effect of curing methods on aggregate properties

3.1.1 Apparent density

Figure 7 presents the apparent density of AAs with various heat and microwave curing regimes. Neither heat nor microwave curing has a noticeable impact on the 28-day apparent density of treated AAs, which remained at around 1700 kg/m^3. The differences between the maximum and the minimum value of heat-cured and microwave-cured AAs are 1.5% and 2.1%, respectively. This fluctuation can be considered as experimental error. Overall, the developed AAs can be classified as

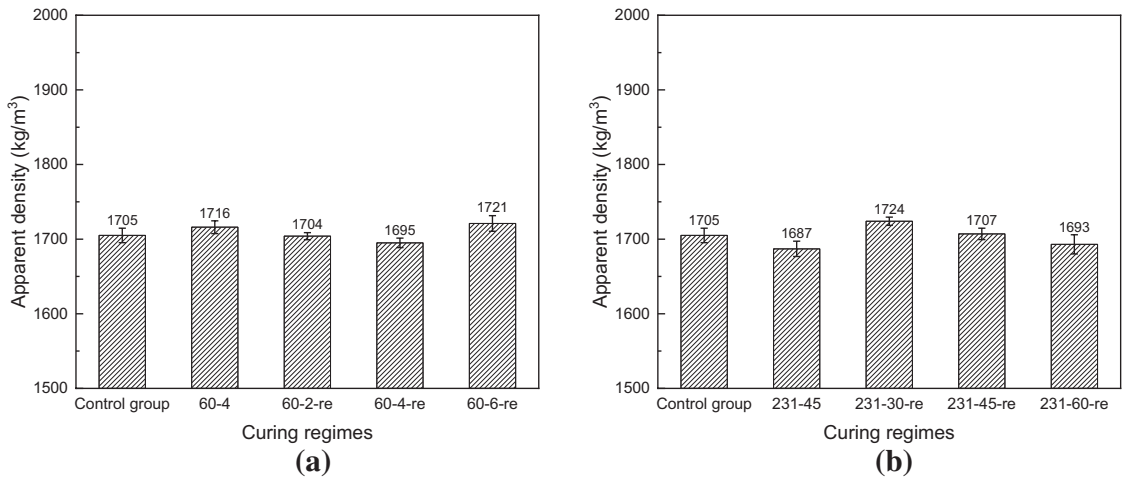

Figure 7 Apparent density of (a) heat-cured and (b) microwave-cured aggregates

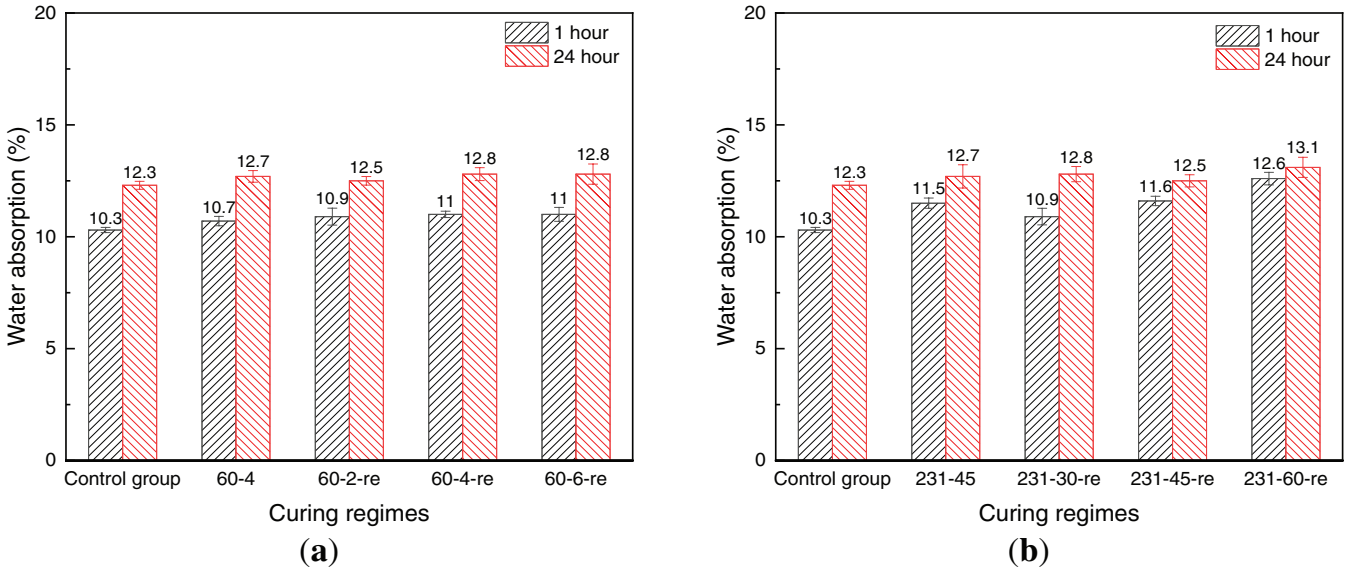

Figure 8 1/24-h water absorption of (a) heat-cured AAs and (b) microwave-cured AAs

lightweight aggregates, as their apparent densities are lower than 2000 kg/m³ [48].

3.1.2 Water absorption

Figure 8 presents the 1-h and 24-h water absorptions of AAs cured under different heating and microwave curing regimes. Heat and microwave curing both increase the 1-h and 24-h water absorptions of AAs slightly. The reason could be that thermal curing could result in the formation of pores and micro-cracks inside the aggregates [1, 2]. The variation of heat curing duration has a marginal impact on the water absorption of AAs, while extending the microwave curing increases their water absorption. This indicates that using the microwave curing method tends to increase the porosity of AAs through water evaporation. It should be noted that even with re-moisturization, the increase in water absorption is not effectively mitigated compared to the control group. This could be due to the irreversible nature of the micro-damage induced by heat or microwave curing [49]. Compared to the AAs prepared with alkali-activated recycled concrete powder in Shen et al. [50], the 24-h water absorption of their samples (around 13%–18%) is moderately higher than that of the present work. Shen et al. [50] further noted that thermal curing effectively reduces the 24-h water absorption, with the minimum value (up to 5% lower than ambient-cured samples) achieved at 60°C curing for 12 h. In contrast, thermal curing exerts a slight negative impact on water absorption in this study. This discrepancy could stem from the high content of inert components (i.e., ES). Thermal curing fails to promote hydration reactions but accelerates water evaporation, potentially inducing internal micro-cracks and thus causing a marginal increase in 24-h water absorption.

3.1.3 Crushing strength

Figure 9 presents the 1-, 3-, 7-, and 28-day crushing strengths of the AAs. Compared to the control group, both heat and microwave curing significantly enhance the early-age crushing strength, improving the 1-day crushing strength by more than 100% and 70%, and the 3-day crushing strength by more than 30% and 20%, respectively. Moreover, extending the heat or microwave curing duration increases the early-age crushing strength. This can be attributed to the effective promotion of reaction product formation by these thermal curing methods at an early stage [20, 51], which will be further discussed in conjunction with microstructural characterisation in the following sections.

However, both heating and microwave curing methods exhibit a negative effect on the 28-day crushing strength of AAs without re-moisturisation. The application of re-moisturisation can mitigate this negative impact to some extent. Specifically, when the heat duration is 4 h or the microwave irradiation duration is 45 s, the application of re-moisturisation enables the 28-day crushing strength comparable to AAs in the control groups. In contrast, either shortening or extending this optimal curing duration would result in lower 28-day crushing strength. The underlying reason is potentially that an insufficient curing duration fails to completely facilitate the reaction, while an excessive duration causes microstructural damage, thereby limiting the strength development [52, 53]. Moreover, the crushing strength of AAs in the current study is also similar to that of AAs prepared with alkali-activated recycled concrete powder [50]. Differently, Shen et al. [50] reported that thermal curing can enhance the 28-day crushing strength, with a maximum improvement exceeding 20% observed at an optimal curing temperature of 60°C. This

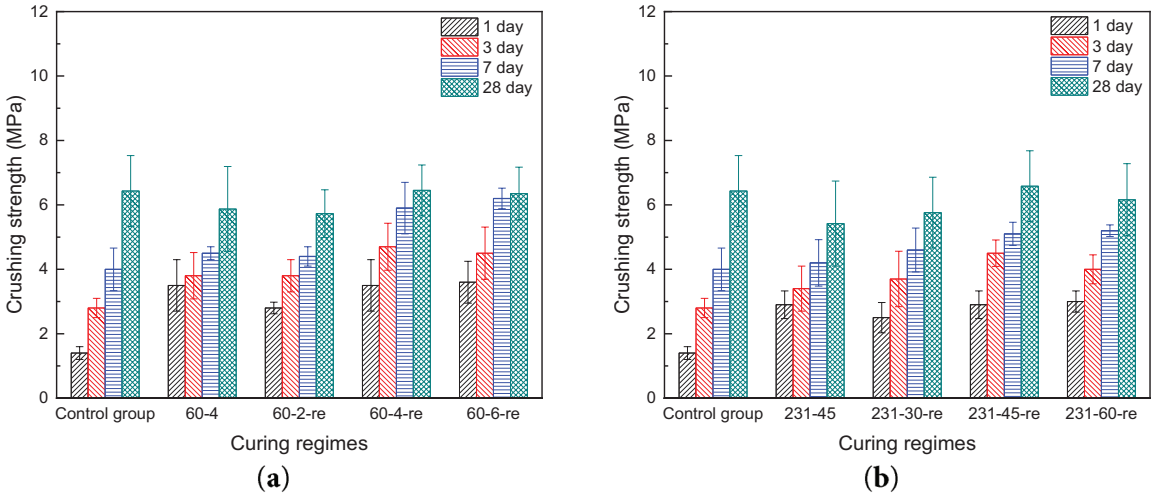

Figure 9 Crushing strength of (a) heat-cured AAs and (b) microwave-cured AAs

discrepancy could be attributed to the high dosage of inert materials incorporated in preparing AAs in the present study.

3.1.4 Thermogravimetric analyses

The thermogravimetric results of AAs cured by heat and microwave radiation after 3 or 28 days are shown in Figure 10. Types of thermal decomposed product can be mainly categorised as C-(A)-S-H gels between 50°C and 220°C and hydrotalcite-like phases between 275°C and 425°C, respectively [16, 54]. The endothermic peaks of calcium carbonates are around 700°C, and the range of calcium carbonate decomposition is between 600 and 750°C [55].

As seen in Figure 10a, 10b, moderate heat and microwave curing can facilitate the reaction with higher amounts of C-(A)-S-H gels and hydrotalcite-like products generated in AAs cured for 3 days compared with the control group. The results agree with the crushing strength result that either heat curing or microwave curing can enhance the 3-day crushing strength. Specifically, prolonging the curing time of heat or microwave curing generally decreases the mass loss corresponding to C-(A)-S-H after 3-day curing, while the values for all heat-cured samples remain higher than

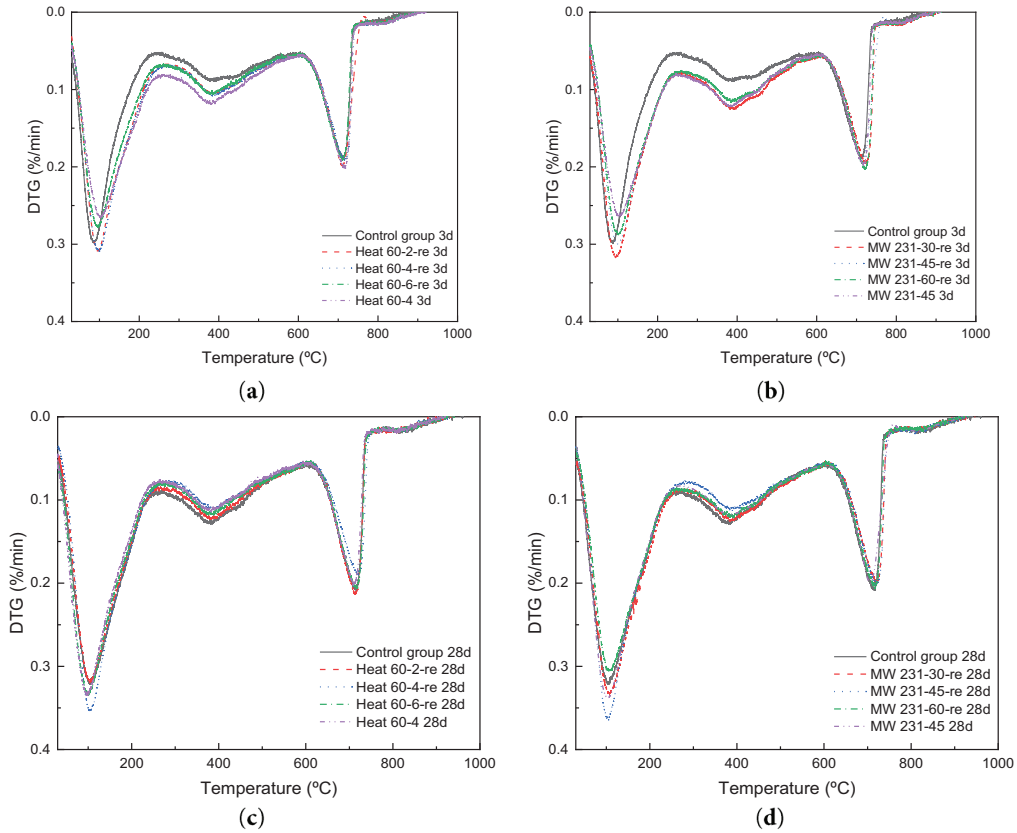

Figure 10 TGA results of AAs with heat curing at the age of: (a) 3-day curing with heat curing; (b) 3-day curing with microwave curing; (c) 28-day curing with heat curing; (d) 28-day curing with microwave curing

those of the control group. This could be caused by the decomposition of the C-(A)-S-H gel under prolonged curing at 60°C [56]. It may contribute to the densification of C-(A)-S-H and thus enhances the material strength to some extent. However, prolonged curing also induces higher shrinkage and consequently leads to coarser pores and microcracks. This offset the positive effects of the densified C-(A)-S-H matrix and finally exerts an adverse impact on strength [57]. This would be the reason that Heat 60-6-re and MW231-60-re exhibit slightly lower 28-day compressive strengths than Heat 60-4-re and MW231-45-re (Figure 9). In terms of hydrotalcite-like phases, an increase in curing time marginally affects the formation of hydrotalcite-like phases for heat curing, while some suspension effect could be observed for microwave curing. This is because heat curing enhances the dissolution of supplementary cementitious materials and subsequently enhances the formation of hydrotalcite-like phases [58]. For microwave curing, although it has a heating effect, the rapid heating may lead to rapid moisture loss, which challenges prolonged hydration and the formation of stable crystalline phases [59]. In general, the strength of the material could be synergistically influenced by multiple hydration products [60]. Additionally, it is observed that re-moisturisation slightly promotes the formation of C-(A)-S-H in AAs at 3 days of age. This can be attributed to the fact that the replenished water can compensate for water evaporation for the ongoing hydration reaction at early stages [61].

Figure 10c, 10d shows the TGA results for the AA samples cured for 28 days. Overall, the mass loss of the C-A-S-H gels reaction products of AAs cured by heat or microwave curing remains at a level comparable to that of the control group. Similar to the results for 3-day curing, insufficient or excessive curing times for heat/microwave treatment, as well as the absence of the re-moisturisation method, could result in a reduced quantity of the C-(A)-S-H gels and therefore weaken the 28-day crushing strength of AAs. Compared with the heat curing, excess microwave curing shows a more obvious negative impact on C-(A)-S-H generation. It corresponds to the slight rise of 24-h water absorption and decline of 28-day crushing strength, since insufficient C-(A)-S-H gels could weaken the compactness of the AA structure. Mass losses of hydrotalcite-like phases for the heat-cured AAs are lower than those of the control group. The reason could be that the heat and microwave curing prevent the further generation of the hydrotalcites. Nevertheless, the heat and microwave curing do not have an obvious influence on the mass loss of calcium carbonates for all the groups.

3.2 Effect of surface treatments on aggregate properties

3.2.1 Apparent density

Figure 11 presents the apparent density of the AAs subjected to various surface treatment methods, including alkaline solution immersion, slurry immersion, and double pelletisation. Compared with the control group (apparent density = 1705 kg/m³), the apparent density of the alkaline solution-treated and double pelletisation-treated AAs increased by 3.83% and 6.22%, respectively. This could be attributed to the densification of the outer layer of AAs. In contrast, slurry immersion had a marginal impact on the apparent density of AAs, with a value of 1706 kg/m³. This reason will be further analysed in conjunction with the results of microstructural characterisation in the following section. Nevertheless, the treated AAs can still be regarded as lightweight aggregates, as their apparent densities are still lower than 2000 kg/m³ [48].

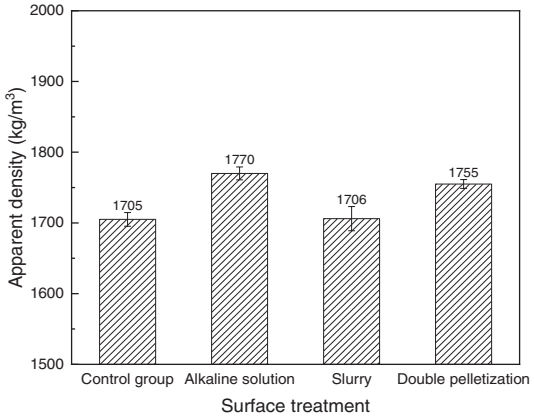

Figure 11 Apparent density of AAs with different surface treatments

3.2.2 Water absorption

Figure 12 shows the 1-h and 24-h water absorptions of AAs treated with different surface modification methods. Both alkaline solution treatment and double pelletisation reduce the 1-h and 24-h water absorptions of AAs. Specifically, the alkaline solution-treated AAs exhibit reductions of 22.3% and 15.0% in 1-h and 24-h water absorptions, respectively. For the double pelletisation treatment, it decreases the 1-h and 24-h water absorptions by 21.5% and 23.8%, respectively. Consistent with the apparent density results in Figure 11, the increase in density is attributed to the formation of a denser outer shell, which results in lower permeability. Similar findings have been reported in previous studies [4, 62]. In contrast, the slurry-treated AAs show an increase in water absorption by 1.79% (1-h) and 6.65% (24-h) compared to the control group, indicating a negative effect of the slurry treatment method. On the one hand, this could be because the additional slurry does not uniformly cover the AAs, and protruding particles increase the surface area, thereby promoting higher water absorption. On the other hand, the higher water content of the slurry tends to cause swelling of the materials [63], leading to increased porosity and thus higher water absorption.

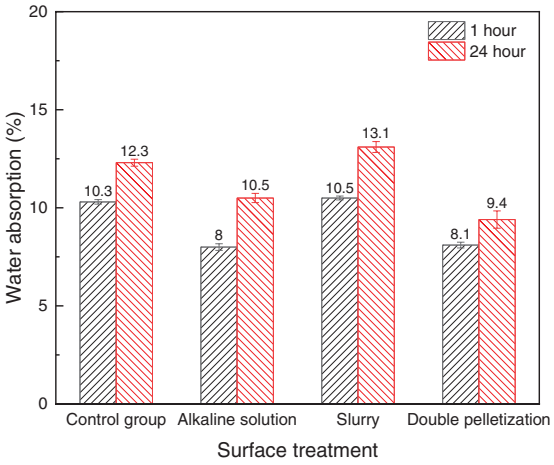

Figure 12 1/24-h water absorption of AAs with different surface treatments

3.2.3 Crushing strength

Figure 13 presents the 7-day and 28-day crushing strengths of AAs considering various surface treatment methods. Compared to the control group, the 28-day crushing strengths of the alkaline solution-treated and double pelletisation-treated AAs increase by 6.2% and 5.9%, respectively. This is because the two surface treatments enhance the outer shell with higher compactness than the internal core. It should be noted that the 28-day crushing strength of slurry-treated AAs decreases by 4.51% compared with the control group. This phenomenon can be attributed to the weakened slurry shell and the protrusions on its surface, which may cause stress concentration and decrease the aggregate load-bearing capacity [64]. This will be further discussed in the following section in conjunction with microstructural characterisation.

3.2.4 Scanning electron microscopy

Figure 14 presents the micrograph of the cross-section of the AAs after different treatments.

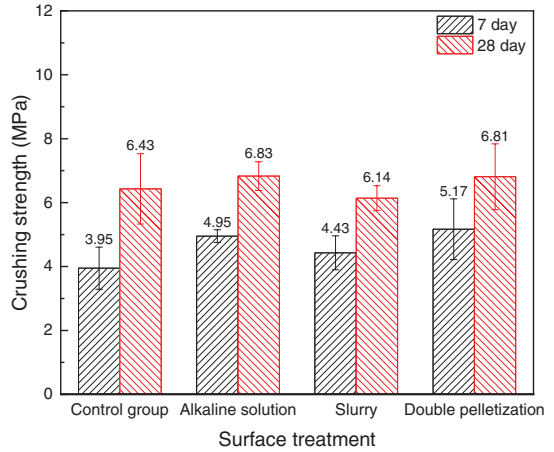

Figure 13 7/28-day crushing strengths of AAs with different surface treatments

On the cross-section of the double pelletisation-treated AA (Figure 14a, 14b), a distinct boundary is visible between the outer shell and the internal core. The outer shell contains a higher concentration of GGBS particles, which are finer and exhibit a lighter, grey-white colour, making the interface easily identifiable. In contrast, no obvious difference is observed between the surface and the core in the alkaline solution-treated AA (Figure 14e). The reason is that the alkaline solution penetrates into the interior of the aggregate rather than forming a distinct new external layer on AA. As for the slurry-treated AA (Figure 14c, 14d), although the interface is less distinct than in the double pelletisation-treated sample, a concentration of finer particles is still evident near the edge of the particle. This is a direct result of the slurry coating process.

A comparison of the SEM images of the three treatment methods reveals that the outer shell formed by double pelletisation exhibits good compactness, despite containing some small voids. In contrast, the near-surface region of the alkaline solution-treated AA is highly compact with almost no voids. Therefore, higher density and lower water absorption were observed for alkaline solution-treated AAs. For the slurry-treated AA, while its edge region also shows relatively high density, the presence of microcracks creates pathways for water ingress, resulting in the increased water absorption shown in Figure 12. This extensive cracking is likely primarily caused by shrinkage induced by the intense reaction between GGBS and the alkali activator, which tends to initiate crack formation.

Upon correlating the SEM results with the 28-day crushing strength results, the slurry-treated AA exhibits the lowest crushing strength among the AAs with surface modifications. This corresponds to its cracked outer shell and surface protrusions, which are prone to stress concentration and consequently lead to reduced crushing strength. In contrast, the other two treatment methods demonstrate improved crushing strength, attributable to the presence of a denser outer shell in AA.

3.2.5 Microhardness

Figure 15 shows the microhardness profiles of the surface-treated AA samples. In the control group, the microhardness remains relatively consistent (50–60 HV) across all measured points from 10 µm to 250 µm. Differently, double pelletisation leads to significantly higher microhardness (60–75 HV) within the outer 10–150 µm region. This increase in microhardness aligns well with the previously observed reduction in water absorption and enhancement in crushing strength. Beyond 150 µm, the microhardness drops to 50–60 HV, matching the control group level, indicating the transition into the unmodified inner core. The microhardness profile further confirms that the reinforced shell thickness is approximately 150 µm,

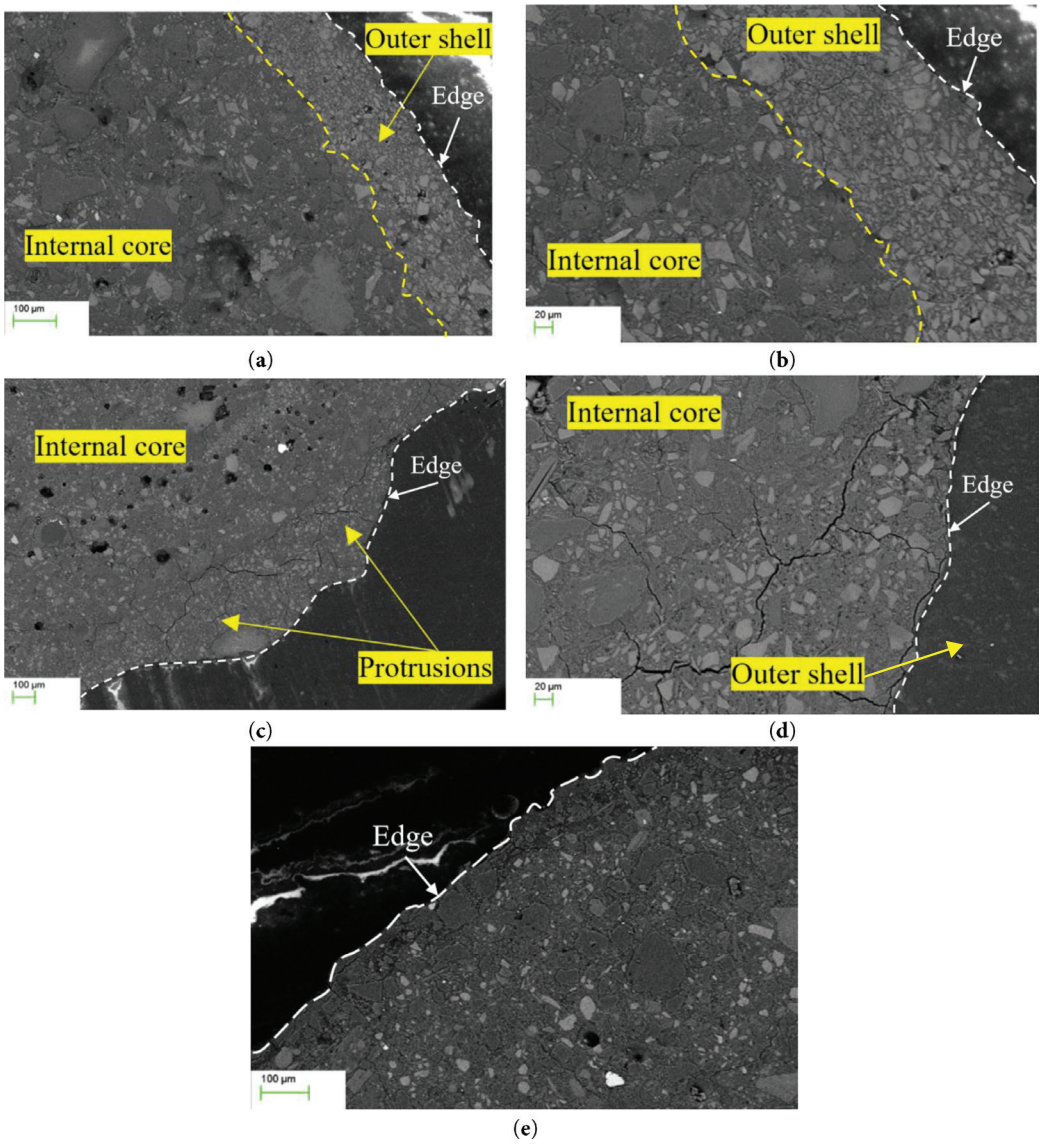

Figure 14 SEM images of AAs treated by: (a,b) double pelletisation, (c,d) slurry, and (e) alkaline solution

consistent with the SEM observations in Figure 14. A similar trend is observed for the alkaline solution-treated AA samples, where the microhardness distribution closely resembles that of the double pelletisation treatment. In contrast, the slurry-treated AA samples exhibit much lower microhardness (25–35 HV) in the near-surface zone (10–70 µm) than in the core zone. The low hardness indicates that the slurry-derived layer lacks sufficient density, which is a key factor contributing to the increased water absorption and reduced crushing strength. This is probably caused by the high water content in the GGBS-based slurry. The microhardness gradually stabilises towards the centre of the aggregate. It is worth noting that the slurry-treated AAs show considerable scatter in microhardness values, which could be attributed to the surface protrusions as well as the microcracks observed near the edge region, as shown in Figure 14. Overall, the alkaline solution treatment and double pelletisation are effective in creating a hard shell for AAs.

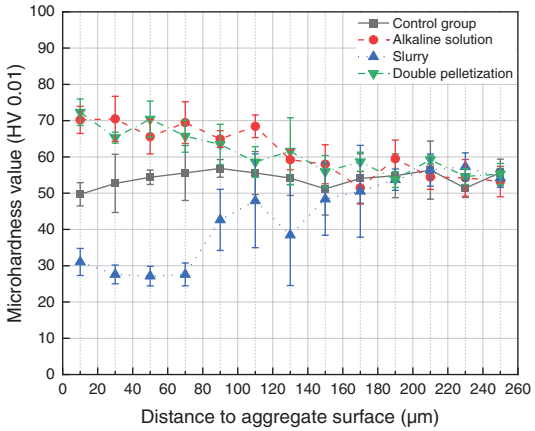

Figure 15 Microhardness values of surface treatment aggregate

4 Conclusions

This paper investigated the effect of various enhancement methods, including heat curing, microwave curing, alkaline solution treatment,

slurry surface treatment, and double pelletisation treatment, on the properties of the alkali-activated soil-based AAs. Apparent density, water absorption, and crushing strength of treated AAs were tested. The influencing mechanisms of these enhancement methods were revealed through microstructural analyses, including TGA, microhardness and SEM. The following conclusions can be drawn:

(1) Heat curing and microwave curing have a marginal impact on the apparent density, but increase the water absorption of AAs slightly. Re-moisturisation during the subsequent curing process provides a negligible mitigating effect, which can be attributed to the irreversible micro-damage induced by the rapid heating process.
(2) Both heat curing and microwave curing significantly enhance the early-age crushing strength of AAs. The effectiveness could be maximised when heating the AAs under 60°C for 4 h or under 231 W microwave heating for 45 s, where the 1-day crushing strength could be improved by more than 140% and 100%, respectively. This enhancement is primarily due to the accelerated alkali-activated reaction and the subsequent increased formation of C-(A)-S-H gels and hydrotalcite. However, maximum reaction product formation does not invariably yield the highest strength, as excessive reaction products under rapid heating tend to induce more microcracks from restrained shrinkage.
(3) Both heat and microwave curing exert negative effects on the 28-day crushing strength of AAs. Although moderate heat or microwave curing enhances the crushing strength through promoting the formation of C-(A)-S-H gels, they may induce microstructural defects to compromise the crushing strength. However, re-moisturisation is found to enhance both early and long-term strengths, which is attributed to its role in promoting the continued formation of C-(A)-S-H gels.
(4) Both alkaline solution treatment and double pelletisation slightly lead to the increased apparent density, reduced water absorption, and enhanced the crushing strength of the AAs. The improvement is mainly attributed to the formation of a dense and hard thin shell covering on the aggregate surface. In contrast, slurry immersion has detrimental effects, decreasing apparent density, increasing water absorption, and reducing crushing strength. This could be primarily attributed to the uneven coating and porous slurry layer.

Although the proposed curing and surface treatment methods can successfully improve the properties of artificial aggregates, their effectiveness in enhancing aggregates performance under complex service environments remains unclear. Future research is needed to investigate the performance degradation of treated artificial aggregates subjected to various environments, such as freeze-thaw cycles, wet-dry alternations, and chemical erosion. Moreover, the deterioration mechanisms in these environments also need to be revealed based on microstructural analyses.

Acknowledgement

This paper is supported by the Ningbo Key Professional Think Tank "Centre for Low Carbon Economy and Scientific Innovation, University of Nottingham Ningbo China".

Funding Statement

Financial support from the Ningbo Municipal Bureau of Science and Technology (Nos. 2023Z148, 2024QL039, 2024Z258) and the Zhejiang Provincial Department of Science and Technology (No. 2025C02257(SD2)) is gratefully acknowledged.

Author Contributions

Shu Liu: conceptualization, methodology, data curation, visualization, writing—original draft preparation; Weixin Zhang: methodology, investigation, data curation, visualization; Yuguang Wang: writing—review & editing; fangying wang: supervision, writing—review & editing; Xiaojian Yu: supervision, writing—review & editing; Binmeng Chen: supervision, writing—review & editing; Bo Li: project administration, funding acquisition, conceptualization, supervision, writing—review & editing. All authors reviewed and approved the final version of the manuscript.

Availability of Data and Materials

The data that support the findings of this study are available from the Corresponding Author, Bo Li, upon reasonable request.

Ethics Approval

Not applicable.

Conflicts of Interest

The authors declare no conflicts of interest.

REFERENCES

[1] Gesoğlu M, Güneyisi E, Öz HÖ. Properties of lightweight aggregates produced with cold-bonding pelletization of fly ash and ground granulated blast furnace slag. Mater Struct. 2012;45(10):1535–46. doi:10.1617/s11527-012-9855-9.
[2] Kayali O. Fly ash lightweight aggregates in high performance concrete. Constr Build Mater. 2008;22(12):2393–9. doi:10.1016/j.conbuildmat.2007.09.001.
[3] Thomas C, Setién J, Polanco JA. Structural recycled aggregate concrete made with precast wastes. Constr Build Mater. 2016;114:536–46. doi:10.1016/j.conbuildmat.2016.03.203.

[4] Chen Y, Zhang Y, Chen T, Zhao Y, Bao S. Preparation of eco-friendly construction bricks from hematite tailings. Constr Build Mater. 2011;25(4):2107–11. doi:10.1016/j.conbuildmat.2010.11.025.

[5] Qian LP, Xu LY, Alrefaei Y, Wang T, Ishida T, Dai JG. Artificial alkali-activated aggregates developed from wastes and by-products: a state-of-the-art review. Resour Conserv Recycl. 2022;177(1):105971. doi:10.1016/j.resconrec.2021.105971.

[6] Perumal G, Sivakumar A. Performance evaluation of alkali activated fly ash lightweight aggregates. Eng J. 2014;18(1):77–86. doi:10.4186/ej.2014.18.1.77.

[7] Masłoń A, Cieśla M, Gruca-Rokosz R, Bichajło L, Nowotnik A, Pytel M, et al. Lightweight artificial aggregates produced from water reservoir sediment and industrial waste-ecological and technological aspect. Materials. 2025;18(11):2563. doi:10.3390/ma18112563.

[8] Almadani M, Razak RA, Al Bakri Abdullah MM, Mohamed R. Geopolymer-based artificial aggregates: a review on methods of producing, properties, and improving techniques. Materials. 2022;15(16):5516. doi:10.3390/ma15165516.

[9] Ibrahim MA, Atmaca N. Cold bonded and low temperature sintered artificial aggregate production by using waste materials. Period Polytech Civ Eng. 2022;67(1):112–22. doi:10.3311/ppci.20885.

[10] Tian K, Wang Y, Hong S, Zhang J, Hou D, Dong B, et al. Alkali-activated artificial aggregates fabricated by red mud and fly ash: performance and microstructure. Constr Build Mater. 2021;281(1):122552. doi:10.1016/j.conbuildmat.2021.122552.

[11] Zhou X, Chen Y, Liu C, Wu F. Preparation of artificial lightweight aggregate using alkali-activated incinerator bottom ash from urban sewage sludge. Constr Build Mater. 2022;341:127844. doi:10.1016/j.conbuildmat.2022.127844.

[12] Zhou X, Tang Z, Zheng Y, Zhang Y, Wu F. Research on the properties and mechanism of a fiber-reinforced alkali-activated lithium slag artificial lightweight aggregate. Constr Build Mater. 2025;472:140866. doi:10.1016/j.conbuildmat.2025.140866.

[13] Liu S, Zhang W, Xu M, Wang F, Hu Y, Li B. Development of cold-bond artificial aggregate with excavated soil and alkali-activated slag. Case Stud Constr Mater. 2024;21(1):e03451. doi:10.1016/j.cscm.2024.e03451.

[14] University BU, Mardani-Aghabaglou A, Özen S, University BT, Gökhan Altun M. Effect of curing conditions during the first 24 hours after casting on the properties of mortar mixtures. Rev de la Construcción. 2020;19(1):68–79. doi:10.7764/rdlc.19.1.68-79.

[15] Koizumi S, Masuda Y. The effects of high temperature curing on hydration reaction and strength development of cement paste containing silica fume at low water binder ratio. J Struct Constr Eng AIJ. 2013;78(685):427–33. (In Japanese). doi:10.3130/aijs.78.427.

[16] Shivaprasad KN, Das BB. Determination of optimized geopolymerization factors on the properties of pelletized fly ash aggregates. Constr Build Mater. 2018;163(1):428–37. doi:10.1016/j.conbuildmat.2017.12.038.

[17] Shivaprasad KN, Das BB. Effect of duration of heat curing on the artificially produced fly ash aggregates. IOP Conf Ser Mater Sci Eng. 2018;431:092013. doi:10.1088/1757-899x/431/9/092013.

[18] Chen W, Li B, Guo MZ, Wang J, Chen YT. Impact of heat curing regime on the compressive strength and drying shrinkage of alkali-activated slag mortar. Dev Built Environ. 2023;14:100123. doi:10.1016/j.dibe.2023.100123.

[19] Sun Y, Zhang P, Hu J, Liu B, Yang J, Liang S, et al. A review on microwave irradiation to the properties of geopolymers: mechanisms and challenges. Constr Build Mater. 2021;294:123491. doi:10.1016/j.conbuildmat.2021.123491.

[20] El-Feky MS, Kohail M, El-Tair AM, Serag MI. Effect of microwave curing as compared with conventional regimes on the performance of alkali activated slag pastes. Constr Build Mater. 2020;233(12):117268. doi:10.1016/j.conbuildmat.2019.117268.

[21] Xu Z, Han X, Feng K, Zhang W, Ma K. Improvement of mechanical properties and microstructure of cementitious materials in a hot-dry environment. Crystals. 2022;12(7):981. doi:10.3390/cryst12070981.

[22] Li S, Xie Y, Zheng X, Liu J, Wang Y, Weng Z. Effect of curing methods on hydration processes and mechanical property of track slab concrete. J Railw Eng Soc. 2023;40(1):103–8.

[23] Wang J, An J, Li Y, Xiang Y, Xiao Q, Tang Z, et al. Influencing factors of the temperature rise of direct electric curing concrete and its effect on concrete properties. Constr Build Mater. 2024;438:137110. doi:10.1016/j.conbuildmat.2024.137110.

[24] Ma C, Dai F, Shi J, Song D, Dong B, Zhou H, et al. Achieving energy savings and early-ages strength enhancement of prefabricated cement components: combined application of direct electric curing and sodium sulphate. J Clean Prod. 2023;425:138802. doi:10.1016/j.jclepro.2023.138802.

[25] Guan X, Luo W, Liu S, Hernandez AG, Do H, Li B. Ultra-high early strength fly ash-based geopolymer paste cured by microwave radiation. Dev Built Environ. 2023;14:100139. doi:10.1016/j.dibe.2023.100139.

[26] Lam TK, Nguyen DT, Le THM, Huynh TP. Effect of microwave curing on the performance of high-volume fly ash concrete. Period Polytech Civ Eng. 2024;68(4):1405–17. doi:10.3311/ppci.37182.

[27] Zhou F, Pan G, Meng H, Mi R. Effect of secondary curing on the performance of microwave cured concrete. Constr Build Mater. 2022;330:127256. doi:10.1016/j.conbuildmat.2022.127256.

[28] Li Q, Wang H, Xue H, Zhang Q, Dong H. The effect of microwave curing on the static and dynamic mechanical properties and thermal brittleness of coal gangue concrete. Constr Build Mater. 2025;463:140025. doi:10.1016/j.conbuildmat.2025.140025.

[29] Uthaichotirat P, Sukontasukkul P, Jitsangiam P, Suksiripattanapong C, Sata V, Chindaprasirt P. Thermal and sound properties of concrete mixed with high porous aggregates from manufacturing waste impregnated with phase change material. J Build Eng. 2020;29:101111. doi:10.1016/j.jobe.2019.101111.

[30] Arjun K, Darshan BU. Synthesis of geopolymer coarse aggregates using class-F fly ash and studies on its physical properties. In: Sustainable Construction and Building Materials: Select Proceedings of ICSCBM. Singapore: Springer Singapore; 2018. p. 155–65. doi:10.1007/978-981-13-3317-0_14.

[31] Pekgöz M, Tekin İ. Microstructural investigation and strength properties of structural lightweight concrete produced with Zeolitic tuff aggregate. J Build Eng. 2021;43:102863. doi:10.1016/j.jobe.2021.102863.

[32] Siletani AH, Asayesh S, Shirzadi Javid AA, Habibnejad Korayem A, Ali Ghanbari M. Influence of coating recycled aggregate surface with different pozzolanic slurries on mechanical performance, durability, and micro-structure properties of recycled aggregate concrete. J Build Eng. 2024;83:108457. doi:10.1016/j.jobe.2024.108457.

[33] Dixit A, Pang SD. Optimizing lightweight expanded clay aggregate coating for enhanced strength and chloride resistance. Constr Build Mater. 2022;321:126380. doi:10.1016/j.conbuildmat.2022.126380.

[34] Colangelo F, Messina F, Cioffi R. Recycling of MSWI fly ash by means of cementitious double step cold bonding pelletization: technological assessment for the production of lightweight artificial aggregates. J Hazard Mater. 2015;299(1):181–91. doi:10.1016/j.jhazmat.2015.06.018.

[35] Colangeloa F, Farinaa I, Pennab R, Feob L, Fraternalib F, Cioffia R. Use of MSWI fly ash for the production of lightweight artificial aggregate by means of innovative cold bonding pelletization technique. Chemical and morphological characterization. Chem Eng Trans. 2017;60(1):121–6. doi:10.1016/j.jhazmat.2015.06.018.

[36] Ferraro A, Ducman V, Colangelo F, Korat L, Spasiano D, Farina I. Production and characterization of lightweight aggregates from municipal solid waste incineration fly-ash through single- and double-step pelletization process. J Clean Prod. 2023;383:135275. doi:10.1016/j.jclepro.2022.135275.

[37] Gesoğlu M, Özturan T, Güneyisi E. Effects of fly ash properties on characteristics of cold-bonded fly ash lightweight aggregates. Constr Build Mater. 2007;21(9):1869–78. doi:10.1016/j.conbuildmat.2006.05.038.

[38] Bekkeri GB, Shetty KK, Nayak G, Dafedar MMM, Jambhale NA, Sachin KC. Waste-derived artificial aggregates for concrete applications. Mater Res Express. 2025;12(8):085306. doi:10.1088/2053-1591/adfd29.

[39] Bekkeri GB, Shetty KK, Nayak G. Producing of alkali-activated artificial aggregates by pelletization of fly ash, slag, and seashell powder. Innov Infrastruct Solut. 2023;8(10):258. doi:10.1007/s41062-023-01227-1.

[40] ISO 14688-2:2017. Geotechnical investigation and testing. Identification and classification of soil. Part 2: principles for classification. London, UK: BSI; 2017.

[41] Magnusson S, Lundberg K, Svedberg B, Knutsson S. Sustainable management of excavated soil and rock in urban areas—a literature review. J Clean Prod. 2015;93:18–25. doi:10.1016/j.jclepro.2015.01.010.

[42] Sun B, Ye G, de Schutter G. A review: reaction mechanism and strength of slag and fly ash-based alkali-activated materials. Constr Build Mater. 2022;326:126843. doi:10.1016/j.conbuildmat.2022.126843.

[43] GB/T 17431.2-2010. Light-weight aggregates and its test methods—part 2: test methods for light-weight aggregates. Beijing, China: Standards Press of China; 2010. (In Chinese).

[44] Alqahtani FK, Rashid K, Zafar I, Iqbal Khan M. Assessment of morphological characteristics and physico-mechanical properties of geopolymer green foam lightweight aggregate formulated by microwave irradiation. J Build Eng. 2021;35(2):102081. doi:10.1016/j.jobe.2020.102081.

[45] Guo W, Zhao Q, Sun Y, Xue C, Bai Y, Shi Y. Effects of various curing methods on the compressive strength and microstructure of blast furnace slag-fly ash-based cementitious material activated by alkaline solid wastes. Constr Build Mater. 2022;357:129397. doi:10.1016/j.conbuildmat.2022.129397.

[46] Luo W, Liu S, Hu Y, Hu D, Kow KW, Pang C, et al. Sustainable reuse of excavated soil and recycled concrete aggregate in manufacturing concrete blocks. Constr Build Mater. 2022;342:127917. doi:10.1016/j.conbuildmat.2022.127917.

[47] Jiang Y, Li B, He J, Garcia Hernandez A. Properties and microstructure of packing-optimised recycled aggregate concrete with different cement paste or sand contents. Constr Build Mater. 2022;344:128178. doi:10.1016/j.conbuildmat.2022.128178.

[48] EN 13055:2016. Lightweight aggregates. London, UK: British Standards Institution (BSI); 2016.

[49] Yim HJ, Park SJ, Jun Y. Physicochemical and mechanical changes of thermally damaged cement pastes and concrete for re-curing conditions. Cem Concr Res. 2019;125:105831. doi:10.1016/j.cemconres.2019.105831.

[50] Shen Z, Zhu H, Meng X. The influence of curing methods on the performance of recycled concrete powder artificial aggregates and concrete. Constr Build Mater. 2024;435:136908. doi:10.1016/j.conbuildmat.2024.136908.

[51] Guo W, Wang S, Xu Z, Zhang Z, Zhang C, Bai Y, et al. Mechanical performance and microstructure improvement of soda residue-carbide slag-ground granulated blast furnace slag binder by optimizing its preparation process and curing method. Constr Build Mater. 2021;302:124403. doi:10.1016/j.conbuildmat.2021.124403.

[52] Dong Z, Ma H, Feng W, Nie Y, Shi H. Achieving superior high-strength geopolymer via the synergistic effect of traditional oven curing and microwave curing. Constr Build Mater. 2022;357:129406. doi:10.1016/j.conbuildmat.2022.129406.

[53] Guntur IN, Tjaronge MW, Irmawaty R, Ekaputri JJ. Compressive strength of medium calcium fly ash based geopolymer paste. IOP Conf Ser Earth Environ Sci. 2020;419(1):012027. doi:10.1088/1755-1315/419/1/012027.

[54] Samantasinghar S, Singh S. Effects of curing environment on strength and microstructure of alkali-activated fly ash-slag binder. Constr Build Mater. 2020;235:117481. doi:10.1016/j.conbuildmat.2019.117481.

[55] De Weerdt K, Sellevold E, Kjellsen KO, Justnes H. Fly ash–limestone ternary cements: effect of component fineness. Adv Cem Res. 2011;23(4):203–14. doi:10.1680/adcr.2011.23.4.203.

[56] Gallucci E, Zhang X, Scrivener KL. Effect of temperature on the microstructure of calcium silicate hydrate (C-S-H). Cem Concr Res. 2013;53:185–95. doi:10.1016/j.cemconres.2013.06.008.

[57] Huang L, An M, Wang Y, Xie Y, Han S, Yu Z. Effect mechanisms of prolonged dry-hot exposure on C-S-H gel properties in cementitious materials. Constr Build Mater. 2025;462:140013. doi:10.1016/j.conbuildmat.2025.140013.

[58] Li B, Tang Z, Huo B, Liu Z, Cheng Y, Ding B, et al. The early age hydration products and mechanical properties of cement paste containing GBFS under steam curing condition. Buildings. 2022;12(10):1746. doi:10.3390/buildings12101746.

[59] Li X, Wang J, Li S, Gao X, Shi Z. Application of low-temperature microwave radiation on the preparation of UHPC. Low Carbon Mater Green Constr. 2025;3(1):3. doi:10.1007/s44242-025-00063-z.

[60] Wang D, Jia H. A quantitative study on the synergistic effect between limestone powder and supplementary cementitious materials. Adv Cem Res. 2022;34(7):324–30. doi:10.1680/jadcr.21.00027.

[61] Cho S, Suh H, Park J, Jeong S, Park J, Bae S. Repetitive water replenishment in CO_2 curing: enhancement in carbon uptake, reactivity, crystal development, and mechanical properties of low calcium binder composites. Cem Concr Compos. 2025;160:106053. doi:10.1016/j.cemconcomp.2025.106053.

[62] Tajra F, Elrahman MA, Stephan D. The production and properties of cold-bonded aggregate and its applications in concrete: a review. Constr Build Mater. 2019;225:29–43. doi:10.1016/j.conbuildmat.2019.07.219.

[63] Alderete NM, Harris MN, Villagrán-Zaccardi Y, De Belie N. Understanding imbibition in cementitious materials including C-S-H strain measurement and geometric restriction. Dev Built Environ. 2025;23:100687. doi:10.1016/j.dibe.2025.100687.

[64] Tajra F, Abd Elrahman M, Lehmann C, Stephan D. Properties of lightweight concrete made with core-shell structured lightweight aggregate. Constr Build Mater. 2019;205:39–51. doi:10.1016/j.conbuildmat.2019.01.194.